



Trace element composition of quartz from alkaline granites – A factor supporting genetic considerations: Case study of the Pitinga Sn–Nb–Ta–Th-cryolite deposit

Karel Breiter^{a,b,*}, Hilton Tulio Costi^c, Michaela Vašinová Galiová^{a,d}, Michaela Hložková^a, Jindřich Kynický^a, Zuzana Korbelová^b, Marek Dosbaba^e

^a BIC Brno, Purkyňova 125, CZ-612 00, Brno, Czech Republic

^b Institute of Geology, Czech Academy of Sciences, Rozvojová 269, CZ-16500 Praha 6, Czech Republic

^c Museu Paraense Emílio Goeldi, CP 8608, 66075-100, Belém, PA, Brazil

^d Institute of Chemistry and Technology of Environmental Protection, Faculty of Chemistry, Brno University of Technology, Purkyňova 118, CZ-612 00, Brno, Czech Republic

^e Tescan Orsay Holding, a.s., Libušina Třída 21, CZ-623 00, Brno, Czech Republic

ARTICLE INFO

Keywords:

Pitinga
Rare metal granite
Peralkaline granite
Quartz chemistry

ABSTRACT

The Madeira pluton, bearing the world-class tin-cryolite deposit of Pitinga, and the closely associated Europa pluton lie in the central part of the Amazon craton, Brazil. The Madeira pluton consists of four principal rock types: early metaluminous porphyritic amphibole-biotite granite with rapakivi texture, metaluminous biotite granite, metaluminous hypersolvus porphyritic granite, and peralkaline albite granite, while the Europa pluton consists of peralkaline riebeckite-biotite alkali feldspar granite. Texture and chemical composition of quartz from all mentioned rock types was evaluated in order: (i) to estimate the contents of trace elements in quartz from peralkaline granites, (ii) to define major differences in the uptake of trace elements into quartz in peraluminous vs. peralkaline conditions, (iii) to better constrain the evolution of the composite Madeira pluton. The contents of Li, Be, B, Na, Al, P, K, Sc, Ti, Mn, Fe, Ga, Ge, Rb, Sr, Zr, Nb, Sn, Sb, Ce, Yb, Hf, Ta, Th, and U in quartz were analyzed using laser-ablation ICP-MS. Quartz from the studied metaluminous and peralkaline granites of the Madeira and Europa plutons is poor in Al (<150 ppm Al) and Li (mostly <20 ppm Li) but enriched in Ge (max. 10 ppm), Sc (max. 6 ppm), and Ga (max. 13 ppm). As suggested by the TitaniQ thermobarometer, the Madeira biotite granite crystallized between ca. 700 and 650 °C at a nearly constant pressure of 3 kbar, while the hypersolvus granite crystallized between 800 and 700 °C at 15–20 to 2 kbar. Textural and chemical data on quartz are in agreement with previous geochronological data: the Madeira pluton comprises two older pulses of less evolved, mostly metaluminous biotite-hornblende and biotite granites, and two younger pulses of mutually mingled metaluminous hypersolvus granite and rare metal-enriched peralkaline albite granite. Differences in texture and composition of quartz do not support direct relations between the hypersolvus granite and the albite granite via magmatic fractionation, but exposure to similar metasomatic processes after their mingling is highly probable. Typical chemical features of quartz from peralkaline granites are relative high contents of Ti and Ge accompanied by low contents of Al and Li, forming an array along the Ti–Ge join in the Ti–Al–Ge ternary diagram.

1. Introduction

The growing consumption of a number of rare metals, also termed “critical raw materials” (European Commission, 2020) or “critical mineral resources” (Schulz et al., 2017) from economic point of view,

has initiated a new wave of interest also in the study of granite-related mineral deposits of Sn, W, Nb, Ta, Li and associated minor components like Rb, Sc, REE, and Th. In order to streamline the search for new granite-related deposits, the conditions of origin of typical well-known and already mined deposits are being re-evaluated using up-to-date

* Corresponding author. BIC Brno, Purkyňova 125, CZ-612 00, Brno, Czech Republic.

E-mail address: breiter@gli.cas.cz (K. Breiter).

<https://doi.org/10.1016/j.jsames.2022.104025>

Received 25 July 2022; Received in revised form 29 August 2022; Accepted 5 September 2022

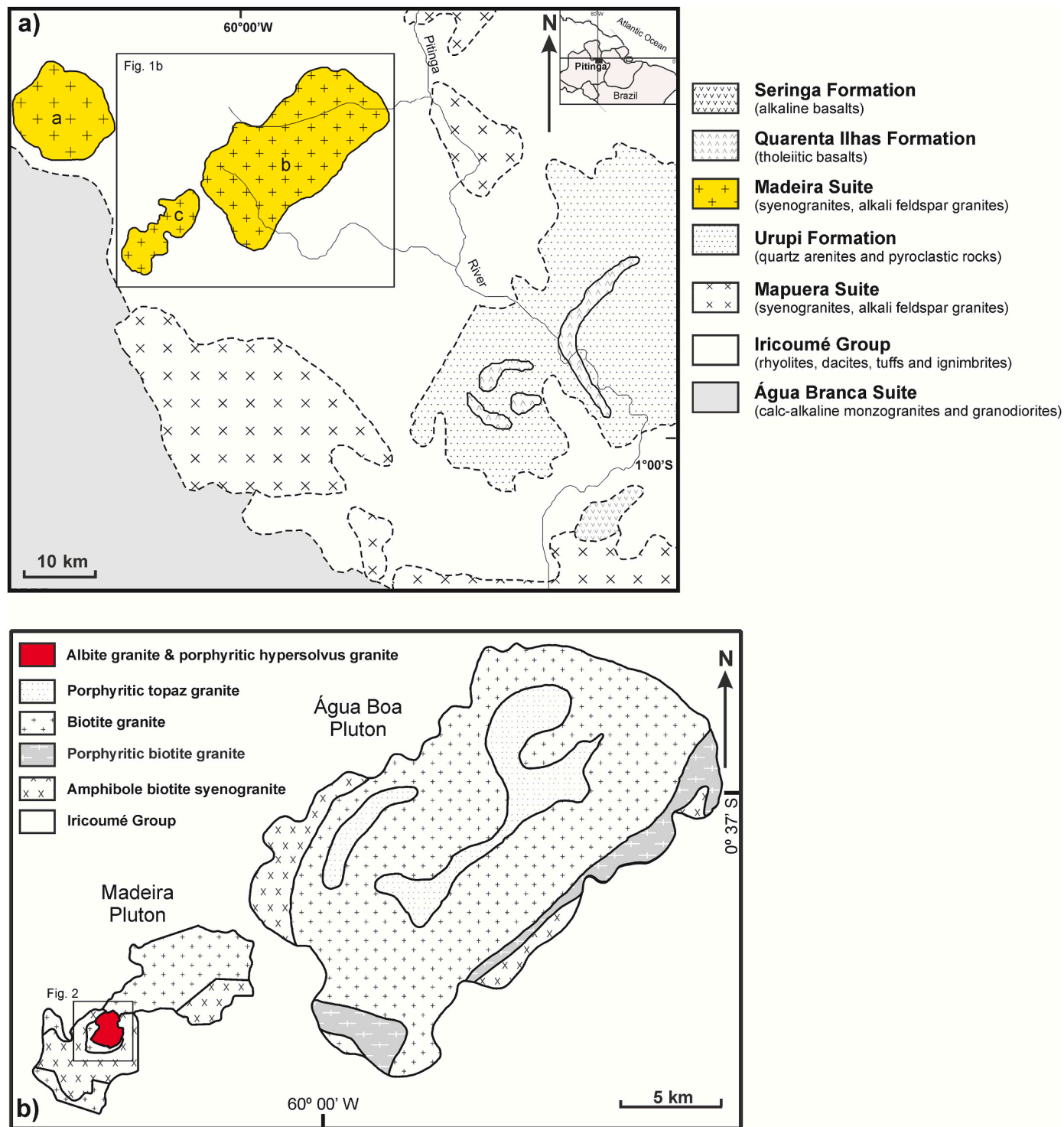
Available online 16 September 2022

0895-9811/© 2022 Elsevier Ltd. All rights reserved.

knowledge and modern laboratory facilities (Breiter et al., 2017; Gourcerol et al., 2019; Marignac et al., 2020; Harlaux et al., 2021; Hreus et al., 2021; Monnier et al., 2021).

The magmatic-hydrothermal evolutionary path of granites and related mineral deposits can be traced, among others, from the chemical composition and the zoning, if present, of rock-forming minerals. Quartz, although being the most abundant component of granites (30–40 vol%) and mostly also the component most resistant to secondary alteration, is still relatively little studied. Only the general

expansion of laser ablation ICP-MS method in Earth sciences in the last two decades yielded first reliable information about trace element contents in quartz. After several pioneering case studies (Larsen et al., 2004; Rusk et al., 2008; Breiter and Müller, 2009; Beurlen et al., 2011; Breiter et al., 2012; Drivenes et al., 2016; Garate-Olave et al., 2017; Monnier et al., 2018; Müller et al., 2018), the first general overview papers were published recently (Breiter et al., 2020; Götze et al., 2021; Müller et al., 2021). Moreover, the use of Ti contents in quartz as a thermo-barometer for granitoids (TitaniQ, Thomas et al., 2010; Huang



and Audétat, 2012) is gaining wider acceptance.

Unlike peraluminous and common calc-alkaline granites, peralkaline granites are still missing data on quartz chemistry. We decided to partly fill this gap and collected data from all evolutionary stages of the unique Sn-cryolite (+Nb, Ta, Th) deposit of Pitinga, Amazon Craton, Brazil. Our aim was to: (i) estimate the contents of trace elements accommodated in quartz from peralkaline granites, (ii) define major differences in the uptake of trace elements into quartz in peraluminous vs. peralkaline conditions, (iii) evaluate the potential of quartz chemistry in constraining the evolution of peralkaline magma.

2. Geological situation and samples

The Madeira pluton, together with the neighboring Água Boa and Europa plutons forming the Madeira suite, are situated in the central part of the Amazon Craton, Amazonas State, Brazil (Fig. 1, Lenharo et al., 2002; Costi et al., 2000a, 2009; Bettencourt et al., 2016). Basement of this area is formed by the Iricoumé Group composed of both effusive and explosive volcanic material of rhyolitic, trachytic, dacitic and andesitic compositions, 1889–1888 Ma in age (Table 1). At ca. 1829–1818 Ma, the Iricoumé Group was intruded by a suite of A-type granites of the Madeira suite including Madeira, Europa and Água Boa plutons. Magmatic evolution of this area was completed at ca. 1780 Ma by the intrusion of dykes and sills of the tholeiitic basaltic rocks of the Quarenta Ilhas Formation (Costi et al., 2000a; Santos et al., 2002; Ferron et al., 2010).

The Madeira pluton (60 km²) consists of four principal rock types (Fig. 2, Table 1; Horbe et al., 1991; Lenharo et al., 2003; Costi et al., 2005, 2009; Bastos Neto et al., 2009). The early mostly metaluminous porphyritic amphibole-biotite granite (1824 ± 2 Ma, Costi et al., 2000a) contains plagioclase-mantled K-feldspar megacrysts, sometimes also reverse-zoned Kfs-mantled plagioclase ovoids and is usually referred to as the “rapakivi granite”. The amphibole-biotite granite was followed by somewhat younger metaluminous biotite granite (1822 ± 2 Ma, Costi et al., 2000a) which contains its xenoliths. Both mentioned granites were later intruded by a sheet-shaped body of peralkaline albite granite, traditionally termed “albite granite facies”. The albite granite body, 2 × 1.3 km in outcrop, is composed of two principal subfacies. The inner (deeper) part of the body is peralkaline, enriched in disseminated cryolite, and contains two major zones composed of thick veins and pods of cryolite and a number of nests of intragranitic cryolite-rich pegmatites (Bastos Neto et al., 2005; Minuzzi et al., 2006; Paludo et al., 2018). The albite granite is, in some parts, strongly enriched in cassiterite, pyrochlore (Costi et al., 2000b, 2002), thorite (Hadlich et al., 2019), and

Table 1

Age and chemical characteristic of magmatic rocks in the Pitinga region. Age of the Quarenta Ilhas Formation according to Santos et al. (2002) by SHRIMP analyzes of zircon and baddeleyite, other ages according to Costi et al. (2000) by single zircon Pb evaporation method.

Geological unit		Chemistry	Age (Ma)
Iricoumé Group		rhyolite, trachyte, dacite, andesite	1889–1888
Madeira Suite	Europa pluton	Rbk-Bt granite	peralkaline
	Madeira pluton	Amp-Bt granite (rapakivi)	metaluminous
		Bt granite	mostly metaluminous
	Hypersolvus granite	mostly metaluminous	1824±2
Albite core granite	rim	peralkaline	1822±2
		metaluminous to peraluminous	1818±2
Quarenta Ilhas Formation		basalt	1780±3

zircon (Nardi et al., 2012). The peralkaline facies is supposed to represent more or less primary magmatic stage of the intrusion and was referred to as the “core facies” (Costi et al., 2009). The outer shell of the intrusion underwent pervasive hydrothermal alteration: it is now metaluminous to slightly peraluminous and contains common fluorite instead of cryolite. In the literature, it is referred to as the “border facies” (Costi et al., 2009). A sheet-like body of mostly metaluminous porphyritic hypersolvus alkali feldspar granite was found outcropping to the west of albite granite; it was reached by several boreholes below the sheet of albite granite. In outcrop, the hypersolvus granite has a smooth or transitional contact with the albite granite, while in boreholes it forms intercalations and interdigitations with it. Similar to the albite granite, the hypersolvus granite from the boreholes shows mostly primary magmatic textural features (sample PHR-191, Fig. 4e), while part of its outcrop was metasomatically altered (sample PHR-176): K-feldspar was partly albitized and silicified (Fig. 4d) and quartz lost CL. Costi et al. (2000a) dated the hypersolvus granite at 1818 ± 2 Ma and, based on interactions along their contact, interpreted the albite and hypersolvus granites to be generally coeval (Costi et al., 2009).

The Europa pluton, located to the NW of the Madeira pluton, is a homogeneous circular body, 90 km² in areal extent, formed by peralkaline hypersolvus riebeckite-biotite alkali feldspar granite with an age of 1829 ± 1 Ma (Costi et al., 2000a). The relatively large Água Boa pluton (350 km²), situated to the NE, consists dominantly of biotite granite with a small proportion of amphibole-biotite granite and topaz-bearing granite (Costi et al., 2005), followed by greisenization and episyenitization with a distinct Sn mineralization (Costi et al., 2002; Borges et al., 2009, 2021).

From chemical point of view, all granites show a typical A-type signature. The amphibole-biotite, biotite and hypersolvus granites, and the metasomatically affected border facies of the albite granite are metaluminous to slightly peraluminous, while the magmatic core facies of the albite granite is peralkaline (Fig. 3a). Potassium prevails over Na in the amphibole-biotite, biotite and hypersolvus granites, while Na strongly dominates over K in the core facies of the albite granite. In the border facies of the albite granite, the Na/K ratio varied according to the grade of metasomatic reworking. Albite granite is strongly but inhomogeneously enriched in F (up to more than 3 wt%), Rb (up to 0.7 wt%), Zr (~0.7 wt%), Sn (~0.2 wt%, Fig. 3b), Nb, Th, Pb, Hf, Y, REE etc. (Costi et al., 2009). Generally, the Madeira pluton can be classified as an A-type rare-metal granite of slightly peralkaline composition.

Nine representative samples from the mineralized Madeira pluton and two from the neighboring Sn-barren Europa pluton were selected for a detailed study of quartz. For sample descriptions see Table 2, for their mineral compositions see Table 3. Localization of all samples and their bulk-rock chemical composition is shown in Electronic Appendix 1 and 2. Textures of all rock types are shown in Fig. 4.

3. Analytical methods

3.1. Automated mineralogy

A TESCAN Integrated Mineral Analyzer (TIMA) based on a TESCAN MIRA FEG-SEM platform in the demonstration facility of TESCAN ORSAY HOLDING in Brno, Czech Republic was used for automated mineralogical, modal and textural analyses. This included collection of backscattered electron (BSE) and energy dispersive (EDS) data on a regular grid of 10 µm point spacing. 1000 counts per pixel were acquired using the high resolution mode. Acceleration voltage of 25 kV and a beam current of 10 nA were used during the data acquisition. The individual points were grouped based on a similarity search algorithm, and areas of coherent BSE and EDS data were merged to produce segments (i.e., mineral grains). Individual spectra from points within each segment were summed. Data from each segment were then compared against a classification scheme to identify the mineral and assign its chemistry and density. The results were plotted as a map showing the

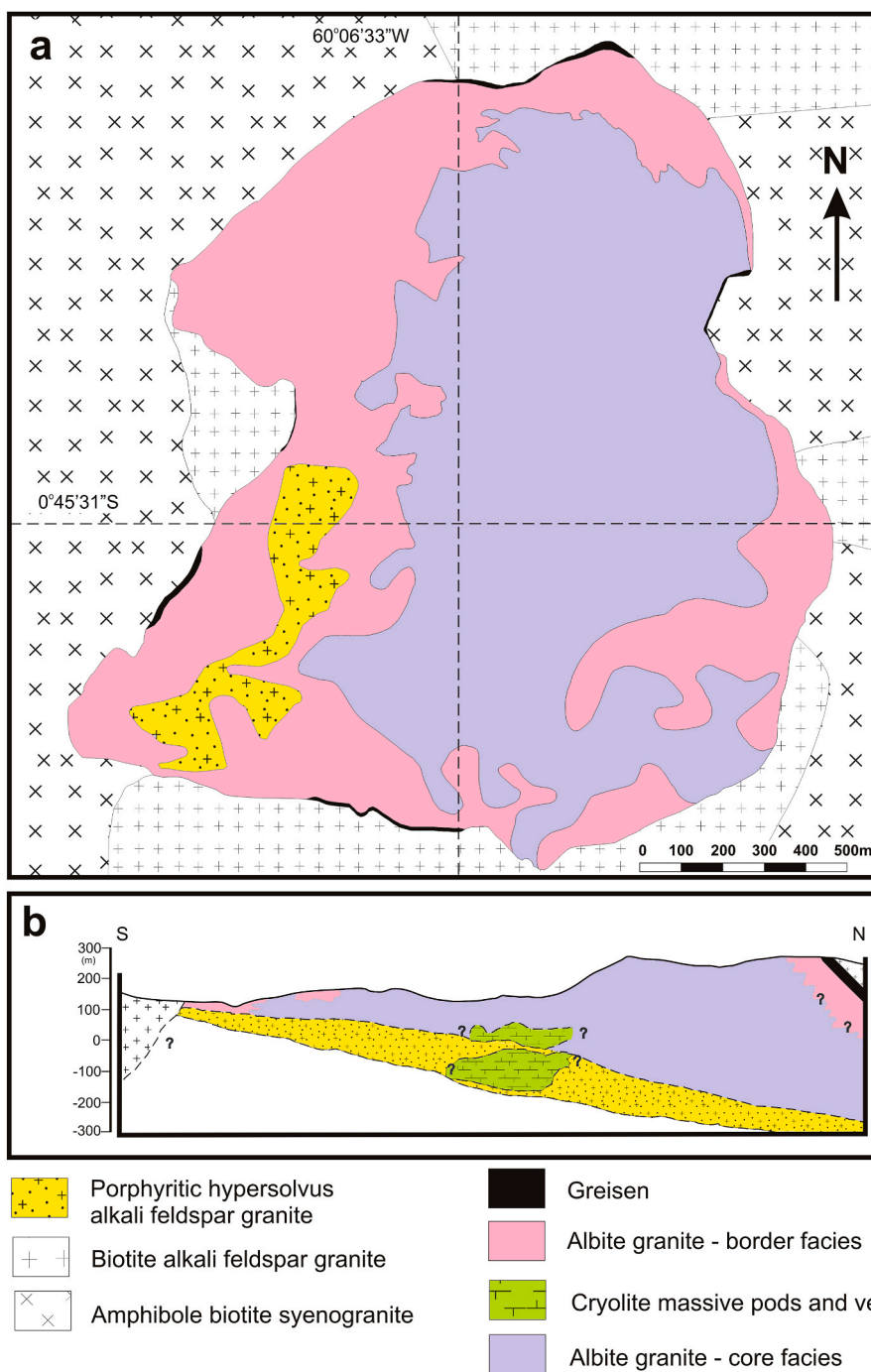


Fig. 2. Detail geological map and section of the Madeira pluton: a, geological map; b, schematic section through the central part of the albite granite body showing the contacts with the early facies and the position of the cryolite-rich zone at the inner core of the albite granite. Vertical scale = horizontal scale (modified from Minuzzi et al., 2006 and Costi et al., 2000a).

distribution of minerals within the sample (Hrstka et al., 2018).

3.2. Cathodoluminescence (CL)

Panchromatic CL images of quartz were obtained using the Jeol JXA - 8230 electron microprobe with a tungsten filament electron source. The images were obtained using a single-channel Panchromatic CL detector - Photomultiplier tube with a wavelength range of 200–900 nm, working distance of 11 mm. The accelerating voltage and current were set to 15 kV and 5–20 nA (according to the intensity of cathodoluminescence). The scanning speed ranged from 100 to 1000 μ s/

pixel depending on the CL emissivity of the imaged area.

3.3. Trace elements in quartz

The contents of trace elements in quartz samples were determined using LA-ICP-MS consisting of quadrupole based ICP-MS (Agilent 7900) connected to the ArF* excimer laser ablation system Analyte Excite+ (Teledyne CETAC Technologies). The laser ablation system emits a laser beam at a wavelength of 193 nm and is equipped with 2-vol Cell HelEx II. The ablated material was carried by He flow (0.5 and 0.3 l min⁻¹) and mixed with Ar (~1 l min⁻¹) prior to entering the ICP mass spectrometer.

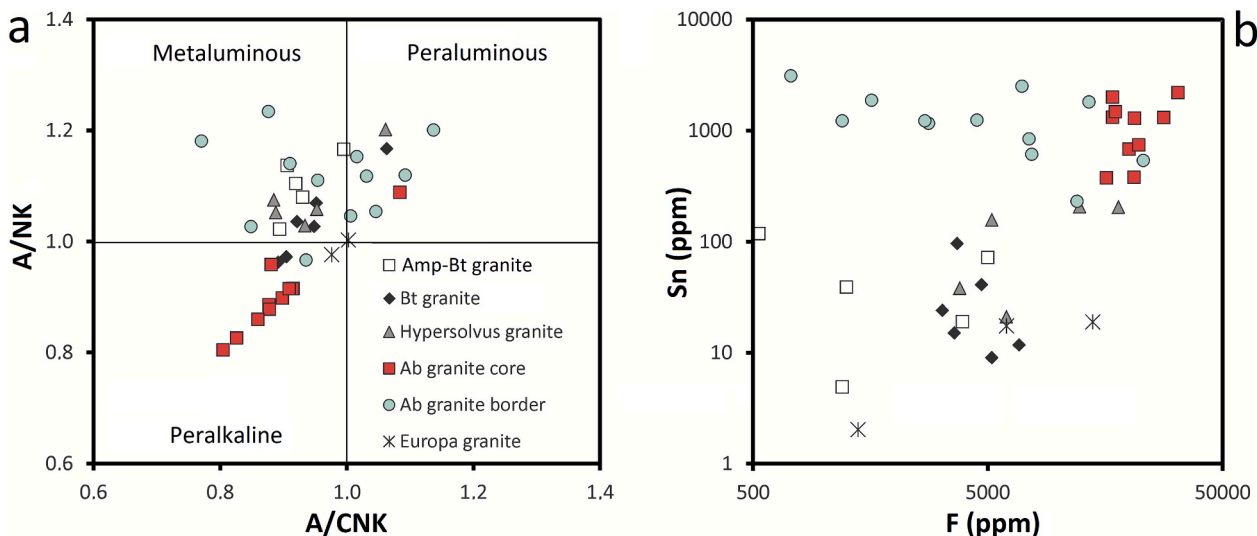


Fig. 3. Geochemical diagrams of Madeira and Europa plutons: a, A/CNK vs. A/NK diagram discriminating peralkaline, metaluminous and peraluminous granites; b, contents of F vs. Sn showing geochemical evolution of granites. Data from Costi et al. (2005, 2009).

The sample surface of individual spots was ablated for 60 s per spot by a 50 μm laser beam diameter with the fluence of 12.7 J cm^{-2} , 10 Hz repetition rate and 60 s washout time. The monitored isotopes are as follows: $^7\text{Li}^+$, $^9\text{Be}^+$, $^{10,11}\text{B}^+$, $^{23}\text{Na}^+$, $^{27}\text{Al}^+$, $^{28,29}\text{Si}^+$, $^{31}\text{P}^+$, $^{39}\text{K}^+$, $^{45}\text{Sc}^+$, $^{47,49}\text{Ti}^+$, $^{55}\text{Mn}^+$, $^{56,57}\text{Fe}^+$, $^{69,71}\text{Ga}^+$, $^{72,73}\text{Ge}^+$, $^{85}\text{Rb}^+$, $^{86,88}\text{Sr}^+$, $^{90}\text{Zr}^+$, $^{93}\text{Nb}^+$, $^{116,117,118,119}\text{Sn}^+$, $^{121}\text{Sb}^+$, $^{140}\text{Ce}^+$, $^{172,173}\text{Yb}^+$, $^{177,178}\text{Hf}^+$, $^{181}\text{Ta}^+$, $^{232}\text{Th}^+$, and $^{238}\text{U}^+$.

ICP-MS was tuned using SRM NIST 612 with respect to the sensitivity and minimum doubly charged ions ($\text{Ce}^{2+}/\text{Ce}^+ < 5\%$), oxide formation ($^{248}\text{ThO}^+ / ^{232}\text{Th}^+ < 0.3\%$) and mass response $^{238}\text{U}^+ / ^{232}\text{Th}^+ \sim 1$. The potential interferences were minimized via a collision cell ($\text{He } 1 \text{ ml min}^{-1}$). The elemental contents were calibrated using artificial glass standards SRM NIST 610 and 612, and Si as the internal reference element after baseline correction and integration of the peak area. For the average detection limits under the operating conditions see Table 4.

Mineral inclusions and large fluid inclusions hidden beneath the sample surface, hence not detectable using BSE and not visible in common ablation-related optical systems, may influence the analytical results, especially so in light elements. To minimize undesirable hits of inclusions, we controlled the target area in a transmitted light mode. Moreover, we believe that occasional hits of relatively large inclusions were eliminated by deleting 10 % of the highest measured values. We concluded that the publication of the 80% dispersion interval of measured values (Electronic Appendix 3) after the elimination of 10 % of the lowest and 10 % of the highest values would be the most correct way of data presentation.

4. Results

4.1. Morphology and CL activity of quartz

The shapes of quartz crystals/grains from the granites of the Madeira Suite are shown in Fig. 4 and their typical CL patterns in Fig. 5. Quartz grains from the Europa riebeckite-biotite granite (Fig. 4a) and from the Madeira biotite granite (Fig. 4c), max. 3 mm and 2 mm in diameter, respectively, are mostly subhedral, scarcely euhedral, indicating their relatively early crystallization. Quartz from the amphibole-biotite granite (Fig. 4b), usually 0.5–2 mm in size, is mostly anhedral, filling the interstices among large feldspar ovoids together with albite and mica. Both facies of the hypersolvus granite, the fresh magmatic from the depth and the metasomatically altered from the surface, contain two distinct types of quartz: relatively large euhedral crystals 2–4 mm in

diameter, and fine anhedral grains in the groundmass (Fig. 4d and e). The albite granite contains large quartz grains, up to 7 mm diameter, with numerous inclusions of small albite laths oriented parallel to the actual surface of the growing quartz crystal (Fig. 4f, g, h). This texture, commonly termed as “snowball”, is typical for crystallization from water- and volatile-rich melt of rare-metal granites (Schwartz, 1992; Müller et al., 2005). Surfaces of these quartz grains are very uneven, with quartz locally invading the surrounding fine-grained feldspars groundmass, locally being resorbed and replaced by albite (Fig. 4g) or K-feldspar (Fig. 4h).

The intensity of quartz CL is highly variable. Well-shaped hexagonal phenocrysts with a regular CL zoning and a strong contrast between individual crystal zones were found in the biotite granite (outcrop, PHR-96, Fig. 5a and b) and in the hypersolvus granite from a deeper part of the pluton (PHR-191) (Fig. 5c and d). Rounded cores rimmed by regularly zoned euhedral rims in some crystals (i.e. Fig. 5d) indicate partial dissolution of quartz due to decompression during ascent of magma from the deep primary reservoir. Note the different style of zoning: dark core + light rim in the hypersolvus granite, and light core + darker rim in the biotite granite.

A less contrasting regular zoning was found in phenocrysts in the amphibole-biotite granite (PHR-101), usually composed of several individual quartz grains (Fig. 5e). Quartz from albite granites is CL-free in all cases. Quartz from the cryolite-rich pegmatite (#4895) forms large multicrystal aggregates that do not allow a CL study due to its dimensions. Quartz from the Europa riebeckite-biotite granite shows a tartan CL pattern and a high density of dark CL-free joins (Fig. 5f).

4.2. Trace elements in quartz

We made altogether 447 spot analyses of quartz from 11 samples. The distribution of some trace elements like Al, Ti, Na, K, Li, Fe, and Mn is inhomogeneous, partially influenced by occasional hits of invisible micro- and nano-inclusions of other mineral and fluid inclusions, and the contents of other traces like Sn, Nb, Ce, Zr, Th etc. are often below detection limits. We therefore decided to present the contents of analyzed elements in the form of medians (Table 4) and intervals of 80% probability (after elimination of 10 % of the lowest and 10 % of the highest analyzed values (Electronic Appendix 3)). These ranges of values are also used in the text. For a better understanding, relations between the genetically most important elements are shown in diagrams (Fig. 6).

The sums of all analyzed trace elements, excluding probable hits of

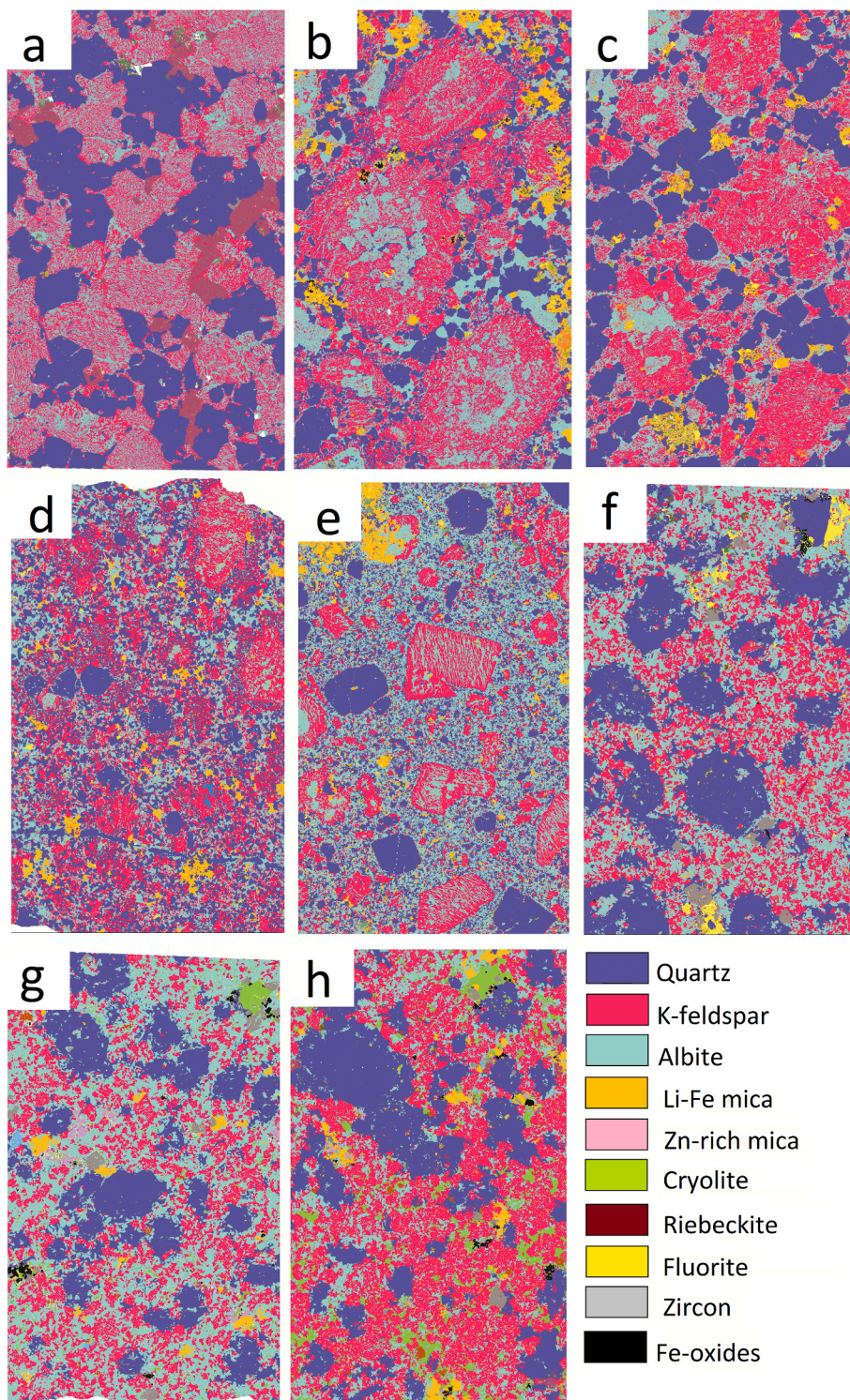


Fig. 4. Rock textures imaged using automated mineralogy mapping (TIMA): a, Europa riebeckite-biotite granite (PHR-195); b, Madeira amphibole-biotite (rapakivi-textured) granite (PHR-101); c, Madeira biotite granite (PHR-96); d, Madeira hypersolvus granite from outcrop (PHR-176); e, Madeira hypersolvus granite from the deeper part of the pluton (PHR-191); f, Madeira albite granite, border facies (PHR-174); g, Madeira albite granite, core facies with Zn-rich mica (PHR-163); h, Madeira albite granite, core facies rich in cryolite (PHR-82 A). Imaged area 30 × 18 mm in all cases.

inclusions, reach 300–500 ppm in the amphibole-biotite and outcropping hypersolvus granites, 150–200 ppm in the core albite granite, and only about 100 ppm in the border facies of the albite granite, cryolite pegmatite and in riebeckite-biotite granite from the Europa pluton. The most common trace elements in the studied quartz are Al, Ti, Li, Na, and K, mostly sharing 70–90 % of the total of all analyzed traces.

Generally, the most common trace element found in Madeira quartz is titanium (Fig. 6a). Its content gradually decreases from ca. 100–200 ppm (medians 147, resp. 160 ppm Ti) in the amphibole-biotite granite and the outcropping hypersolvus granite, across 28–103 ppm (median

66 ppm Ti) in the biotite granite and 26–57 ppm (median 41 ppm Ti) in the deep hypersolvus granite to less than 10 ppm (medians <5 ppm Ti) in albite granite and pegmatite samples. In Europa granites, 22–58 ppm (median 34 ppm) of Ti was found.

The content of Al is slightly higher in the amphibole-biotite, biotite and hypersolvus granites with medians in the range of 100–127 ppm Al than in the albite granite (medians 96 and 82 ppm Al in the core and border facies, respectively) and cryolite pegmatite (median 47 ppm Al). Individual spots with 150–350 ppm Al were found especially in the biotite granite; Al content at these spots does not correlate with K or Na

Table 2
Basic description of studied quartz samples.

Sample No.	Coordinates	Rock description	Localization	Shape of the larger quartz grains	CL activity of quartz
PHR-101	0°45'12"S 60°07'23"W	Amphibole-biotite granite, coarse grained, porphyritic, rapakivi texture	Madeira pluton, outcrop	Subhedral to anhedral grains	Multiply indistinct zoning in light shades
PHR-96	0°46'25"S 60°08'36"W	Biotite granite, medium grained, red coloured	Madeira pluton, outcrop	Well-shaped hexagonal phenocrysts	Strong zoning, bright core + dark rim
PHR-176	0°45'25"S 60°06'53"W	Hypersolvus alkali feldspar granite, medium grained, light gray	Madeira pluton, outcrop	Generally hexagonal grains. Edges in detail uneven, invading surrounding matrix	No CL-activity
PHR-191	0°45'27"S 60°06'28"W	Hypersolvus alkali feldspar granite, fine-grained porphyritic, dark gray	Madeira pluton, borehole 250 S/750 W, depth 150.8 m	Well-shaped hexagonal phenocrysts	Strong zoning, dark core + lighter rim
PHR-174	0°45'24"S 60°06'41"W	Albite granite, border facies, medium grained, dark brown-red coloured	Madeira pluton, outcrop	Rounded grains containing numerous Ab-inclusions. Edges in detail uneven, invading surrounding matrix	No CL-activity
PHR-127	0°45'14"S 60°06'40"W	Albite granite, core facies, fluidal, medium grained, light gray in colour	Madeira pluton, outcrop	Rounded grains with Ab-inclusions, without clear border passing into matrix	No CL-activity
PHR-82 A	0°45'09"S 60°06'19"W	Albite granite, core facies, medium grained, dark gray	Madeira pluton, outcrop	Rounded grains with Ab-inclusions, locally from border replaced by feldspars	No CL-activity
PHR-163	0°45'19"S 60°06'19"W	Albite granite, core facies, medium grained, gray	Madeira pluton, borehole 00/400 W, depth 99.1 m	Rounded grains containing numerous Ab-inclusions. Edges in detail uneven, invading surrounding matrix	No CL-activity
4895	0°45'18"S 60°06'38"W	Pegmatite with black cryolite	Pitinga, mine	Large uneven grains	
PHR-195	0°37'01"S 60°09'26"W	Hypersolvus riebeckite-biotite granite, medium grained, light red in colour	Europa pluton	Uneven to subhedral grains, scarce feldspar inclusions	Generally light, some grains multiply indistinctly zoned other with tartan or patchy texture. CL disappears along abundant joins.
PHR-197	0°38'24"S 60°09'59"W				

Table 3
Mineral composition (TIMA) of studied samples (wt%).

Sample No.	PHR-195	PHR-96	PHR-101	PHR-176	PHR-191	PHR-163	PHR-82	PHR-127	PHR-174	4895
Rock	Europa Rbk-Bt granite	Madeira Bt granite	Madeira Amp-Bt granite	Madeira hypersolv. granite	Madeira Ab granite core			Madeira Ab granite border	Madeira Crl pegmatite	
Quartz	34.22	34.14	26.74	34.82	27.92	25.82	25.68	20.58	29.83	62.77
K-feldspar	32.16	37.73	33.04	31.4	29.1	25.33	35.7	35.41	26.84	0.17
Albite	27.25	22.74	29.66	27.39	35.86	37.67	24.25	35.61	37.96	0
Cryolite	0	0	0	0	0.08	2.67	6.28	1.72	0	34.0
Fe-Li-mica	0.64	3.83	6.34	5.14	4.50	1.80	3.58	1.96	0.96	0
Zn-rich annite	0	0	0.01	0.01	0.13	0.90	0.15	0.01	0	0
Riebeckite	4.75	0	0	0	0.51	0.36	0.91	0.1	0	0.02
Zircon	0.16	0.10	0.14	0.10	0.19	1.04	1.51	0.50	1.77	0
Fluorite	0.03	0.67	0.56	0.51	0.46	0.02	0.03	0.01	0.82	0.05
Fe-oxides	0.02	0.01	0.50	0.01	0.10	0.53	0.58	0.17	0.87	0
Ti-oxides	0.07	0	0.67	0.07	0.08	0	0	0	0	0
The rest	0.70	0.78	2.34	0.55	1.07	3.86	1.33	3.93	0.95	2.63

contents and, as such, should not be explained as hits of feldspar nanoinclusions. The Europa granite contains 16–89 ppm (median 52 ppm) Al.

Between alkalis, potassium slightly prevails over sodium in quartz from the deeper hypersolvus granite (medians 37 vs. 18 ppm) and in the border albite granite (medians 18.5 vs. 7.5 ppm), while Na prevails over K in quartz from the amphibole-biotite (medians 27 vs. 9 ppm), biotite (medians 16 vs. 8 ppm), outcropping hypersolvus granite (medians 98 vs. 29 ppm) and in the pegmatite (medians 46 vs. 15 ppm). The contents of the two alkalis are similar in quartz from all samples of the core albite granite (medians 30–62 ppm Na vs. 39–52 ppm K). In quartz from the Europa granite, the contents of both alkalis are comparatively low: 9 ppm Na and 8 ppm K.

The content of lithium in quartz is relatively low: the highest was found in the amphibole-biotite granite (11–28, median 22 ppm), the lowest in the pegmatite (median 1.1 ppm Li) and in the border albite granite (median 0.8 ppm Li, Fig. 6b).

Ga, Ge and Sc are relatively scarce elements in granitoids (ca. 18, 1.3 and 5 ppm, respectively, Shi et al., 2011), chemically similar to Al, Si and Fe, usually dispersed in rock-forming minerals (Breiter et al., 2013). A notable enrichment in Ge was found in quartz from the albite granite (range 1.5–5.3 ppm, medians of individual samples 3.6–4.8 ppm Ge) and notably from the pegmatite (6.4–9.4 ppm, median 8.3 ppm Ge). In other granites, medians between 0.8 and 1 ppm were found (Fig. 6c). The content of Ga is much lower, lying in the range of 0.02–0.06 ppm. The only exception is quartz from pegmatite, containing 0.06–5 ppm (median 1.2 ppm) Ga (Fig. 6d). Scandium shows, compared to all other studied elements, the lowest dispersion within each quartz sample. The highest contents were found in quartz from the border albite granite and the neighboring hypersolvus granite (medians 4.4, resp. 3.8 ppm Sc), while the core albite granite and the deeper hypersolvus granite contain quartz with 2.4 and 1.8 ppm Sc. The amphibole-biotite and biotite granites and pegmatite contain quartz with only 0.20–0.28 ppm Sc (Fig. 6e).

Table 4
Medians of trace-element contents in quartz (ppm) (bdl-below detection limit).

	limit of detection	PHR-197	PHR-195	PHR-101	PHR-96	PHR-176	PHR-191	PHR-174	PHR-127	PHR-163	PHR-82 A	4895
Rock		Europa Rbk-Bt granite		Madeira Amp-Bt granite	Madeira Bt granite	Madeira hypersolv. granite		Madeira Ab granite border	Madeira Ab granite core			Madeira CrI pegmatite
Li	0.73	4.85	1.78	22.1	3.18	5.73	13.4	0.8	10.67	10	11	1.12
Be	0.44	bdl	bdl	bdl	bdl	0.52	bdl	0.8	bdl	bdl	0.45	bdl
B	2.2	bdl	bdl	bdl	bdl	bdl	bdl	bdl	bdl	2.2	bdl	3.67
Na	7.0	7	17	27	16	98	19	8	30	62	34	46
Al	1.03	65	24	124	127	117	100	82	95	92	103	46
P	19	22	bdl	bdl	33	bdl	21	bdl	24	bdl	bdl	bdl
K	4.5	bdl	12	9	8	29	37	19	39	42	52	15
Sc	0.12	2.6	3	0.3	0.2	3.8	1.8	4.4	4.7	0.3	2.4	0.3
Ti	0.36	30	34	147	66	160	41	5	5	2	4	1
Mn	0.23	bdl	0.7	1	0.4	1.2	0.4	bdl	bdl	0.3	bdl	0.3
Fe	1.3	3.1	2.2	14.8	3.4	23.4	1.9	3.1	3.9	8.7	5.8	5
Ga	0.02	0.02	0.02	0.03	0.03	0.02	0.4	0.04	0.04	0.06	0.26	1.22
Ge	0.55	0.99	0.98	0.86	0.9	0.79	1.05	4.28	4.78	3.64	3.64	8.28
Rb	0.03	bdl	0.58	0.14	0.12	0.69	1.3	3.44	1.27	2.25	6.65	1.03
Sr	0.014	0.13	0.08	0.11	0.02	bdl	0.2	1.21	1.15	3.16	0.14	1.66
Zr	0.005	0.03	1.0	0.05	0.02	0.06	0.02	0.15	0.08	0.05	0.06	0.01
Nb	0.004	0.06	0.05	bdl	bdl	1.12	0.01	0.28	0.21	6.0	0.02	bdl
Sn	0.07	bdl	0.08	0.07	bdl	1.02	0.09	0.25	0.24	0.09	0.1	0.1
Sb	0.14	bdl	bdl	bdl	bdl	bdl	bdl	bdl	bdl	bdl	bdl	bdl
Ce	0.002	0.04	0.01	0.01	bdl	0.04	bdl	0.01	0.01	0.01	bdl	0.01
Yb	0.008	0.01	0.01	bdl	bdl	0.01	0.01	0.01	0.01	bdl	0.01	bdl
Hf	0.004	bdl	bdl	bdl	bdl	0.01	0.01	0.02	0.01	bdl	0.01	bdl
Ta	0.001	bdl	bdl	bdl	bdl	bdl	bdl	0.01	bdl	bdl	bdl	bdl
Th	0.002	0.01	4	bdl	bdl	0.01	0.01	2.3	0.9	0.55	1.34	1.31
U	0.002	bdl	bdl	bdl	bdl	0.01	0.01	bdl	bdl	0.01	bdl	bdl

The highest contents of Fe and Mn were found in quartz from the outcropping hypersolvus and the amphibole-biotite granites (23 and 15 ppm Fe vs. 1.2 and 1 ppm Mn); quartz from other granites contains max. 5.2 ppm Fe and 0.38 ppm Mn as medians.

Among other elements, we should mention the slight enrichment in B in quartz from the pegmatite (median 3.7 ppm), enrichment in Rb in quartz from the albite granite (medians 3.4 ppm in the border and 1.3–6.6 ppm in the core facies), enrichment in Sr in quartz from the albite granite and pegmatite (medians 0.74 and 1.55 ppm Sr), enrichment in Nb and Sn (Fig. 6f) in quartz from the outcropping hypersolvus granites (median 1.12 ppm Nb, 1.02 ppm Sn), and the enrichment in Th in quartz from the border albite granite and pegmatite (medians 2.3 and 1.3 ppm Th, respectively). The contents of other analyzed elements Zr, Hf, Ta, Ce, Yb, and U in quartz only scarcely exceed 0.1 ppm at some spots.

4.3. Chemical zoning of quartz crystals

Some quartz crystals from Madeira pluton exhibit a distinct CL and chemical zoning. Real cause of cathodoluminescence of quartz and its relation to chemical zoning is still rather controversial issue (Perny et al., 1992; Rusk et al., 2006; Götze, 2009). Nevertheless, strong CL of magmatic quartz usually corresponds to Ti-enrichment in quartz crystallizing at higher temperatures (i.e. in rhyolites), while weak to none CL is common in low-temperature (but still magmatic) quartz or hydrothermally equilibrated quartz (for example greisen quartz).

In case of chemical zoning of studied quartz grains, zoning of Ti is the most intense and, moreover, corresponds well with the CL pattern: domains with higher Ti contents have higher intensities of CL, i.e., are relatively bright. The contents of Ti decrease from core to rims (100–150 → 25 ppm Ti) in quartz crystals from the biotite granite (Fig. 7a) but increase from core to rims (ca. 11 → 40 ppm Ti) in crystals from the hypersolvus granite (Fig. 7b). Quartz from the amphibole-biotite granite shows no regular chemical zoning (Fig. 7c). A remarkable zoning in trace elements Li and Sn was found in quartz from both facies of the albite granite, in all cases with relative enrichments in crystal cores (Fig. 7d and e).

5. Discussion

5.1. Specific features of quartz from peralkaline granitoids

Chemical composition of quartz from peralkaline granitoids has not been published yet. To establish chemical features typical for peralkaline quartz, we compared our data from the Madeira and Europa plutons with already published large datasets from strongly peraluminous (S-type) and metaluminous (A-type) granites (Fig. 8).

Chemistry of quartz from the metaluminous Madeira amphibole-biotite and biotite granites is similar to that from classical pyterlite from the Wiborg batholith, Finland, and from less evolved biotite A-type granites from the Sn-deposit of Cínovec/Zinnwald, Erzgebirge (Breiter et al., 2020). It is characterized by relatively high Ti and low Al contents (100–250 ppm and 100–150 ppm, respectively), a positive correlation between Al and Ti, 20–30 ppm Li, and max. 1 ppm Ge. Quartz from the peralkaline Madeira granites tends to be even poorer in Al, usually containing <150 ppm Al, with the lowest values in the cryolite pegmatite with medians near 50 ppm. These low Al contents differ from already published median Al contents in quartz from A-type and S-type granites (160 ppm and 447 ppm Al, respectively; Breiter et al., 2020) and from granite-related pegmatites (100–1000 ppm Al; Müller et al., 2021) (Fig. 8a).

Quartz from the clearly peralkaline Europa granite is even poorer in Al (15–90 ppm) and is similar to quartz from strongly peralkaline granites like Khan Bogd, Mongolia in its composition (unpublished author's data, for geological characteristics see Kovalenko et al., 2006).

Already Jacamon and Larsen (2009) assumed that the Al-content in quartz should correspond to amount of Al available in the melt, i.e. positively correlate with the aluminum saturation index (ASI). Something later, Breiter and Müller (2009) disputed this idea founding extreme high Al-content also in magmatic quartz from strongly evolved subaluminous granites at Hora Svaté Kateřiny, Erzgebirge. Nevertheless, generally lower content of Al in quartz from subaluminous A-type granites in comparison with peraluminous S-type granites was statistically proved (Breiter et al., 2020). The very low-contents of Al found in peralkaline granites from the Madeira and Europa plutons, including the

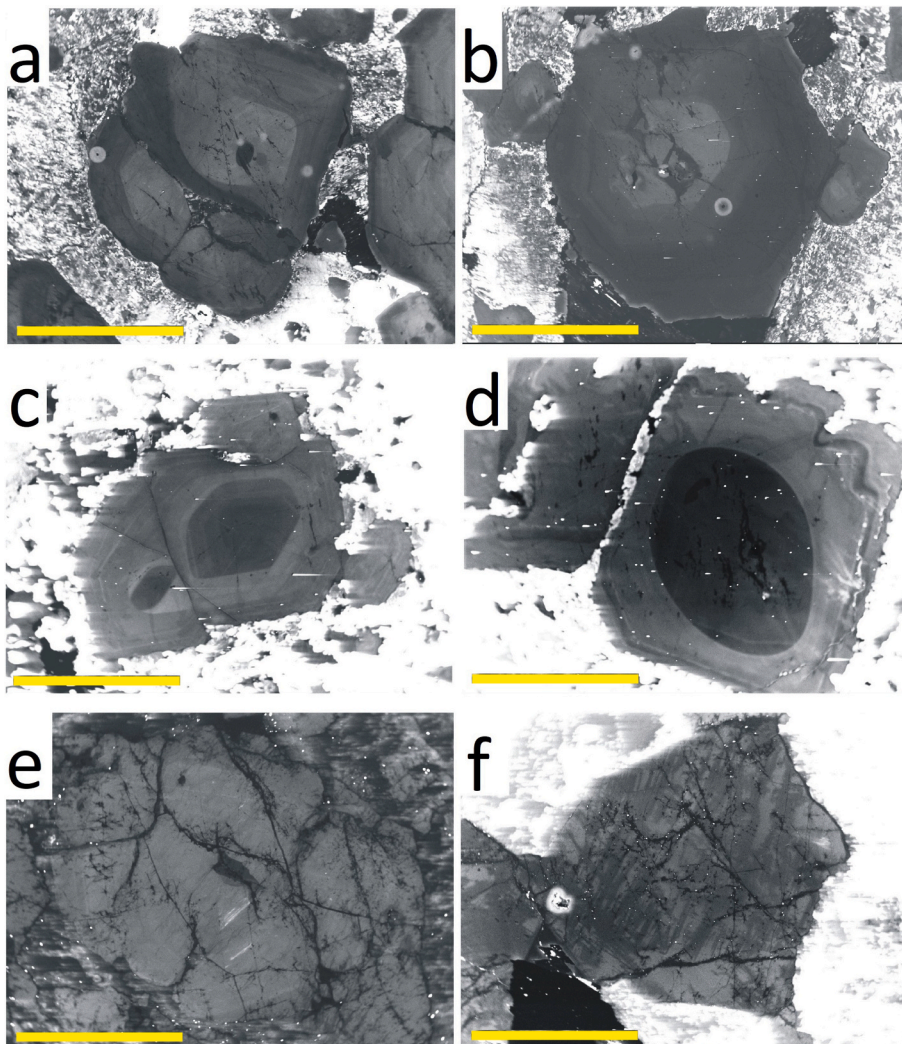


Fig. 5. Cathodoluminescence textures of quartz: a, and b, zoned quartz phenocrysts from Madeira biotite granite (PHR-96) with relatively light cores and dark rims; c, and d, well-shaped quartz phenocrysts from the Madeira hypersolvus granite (PHR-191) with relatively dark cores and light rims. Two adhered cores on fig. c indicate joining of quartz crystals during ascent of magma, while the rounded core on fig. d proves partial dissolution of quartz crystals during this movement; e, quartz crystal in the Madeira amphibole-biotite granite (PHR-101) is CL-homogeneous; f, irregularly patchy-textured quartz from the peralkaline Europa granite (PHR-197). Scale bars 1 mm in all cases.

strongly geochemically evolved members like the albite granite and cryolite pegmatite, confirm the validity of the original idea of [Jacamon and Larsen \(2009\)](#).

The low Li contents in the Pitinga quartz, mostly <20 ppm, are consistent with the generally lower Li contents in quartz from metaluminous A-type granites compared with granites of S-type (15 vs. 30 ppm Li; [Breiter et al., 2020](#)). While Li accommodates free spaces in the quartz structure as the most important valence compensator for Al ($\text{Al}^{3+} + \text{Li}^+ \leftrightarrow \text{Si}^{4+}$) ([Götze et al., 2021](#)), the uptake of Li in quartz is limited by the available number of Al^{3+} ions in the structure, i.e., the Al content in quartz. Theoretically, the atomic Li/Al ratio cannot be greater than one and in fact, we found only several spots not respecting this condition ([Fig. 6b](#)). This feature limited the entry of Li in quartz also in Li-rich varieties of peralkaline and metaluminous granites ([Fig. 8b](#)).

Gallium is a relatively common (Earth average 19 ppm, [www.webelements.com](#)) but dispersed trace element, chemically similar to Al. Information about Ga in quartz is scarce: only [Müller et al. \(2021\)](#) reported unique contents up to 5 ppm Ga in quartz from LCT-type pegmatites, also containing hundreds of ppm Al (i.e., Al/Ga~100). The Al/1000 Ga values in granites range between 2 and 4, decreasing to 1, i.e., Al/Ga~1000 in highly fractionated granites (see review in [Breiter et al., 2013](#)) including the Madeira albite granite. Nevertheless, the enrichment in Ga to about 0.06 and 1.2 ppm (medians) in quartz from the Madeira albite granite and cryolite pegmatite, respectively, along with the low Al contents of 96 and 46 ppm (medians), respectively, resulted in unusually low Al/Ga values of 70, resp. 38. This indicates a preferred

uptake of Ga into the quartz lattice in peralkaline environment, but further research will be necessary to fully understand this process. It is worth noting that Ga is usually dispersed in Al-bearing phases; therefore, the very low Al contents in Ga-enriched quartz exclude occasional hits of Al, Ga-bearing minerals by laser ablation.

The enrichment in Nb and Sn of quartz from the hypersolvus granite (medians 1.12 and 1.02 ppm, respectively) and the enrichment in Th of quartz from the albite granite and cryolite pegmatite (medians between 0.7 and 2.3 ppm) also seem to indicate an entry of these elements into the quartz lattice. A great majority of analyses of these samples yielded values well above the detection limits. The Nb/Sn ratio here is ca. 1:1, which does not correspond to any known Nb, Sn-mineral, i.e., these values do not represent accidental hits of inclusions.

Typical features of quartz from peralkaline granites are well constrained in the Ti–Al–Ge ternary diagram ([Fig. 8c](#)), forming an array along the Ti–Ge join.

5.2. Estimation of conditions of quartz crystallization

Ti zoning is herein used for an approximate calculation of pressure-temperature (P-T) paths of Madeira granites using the TitaniQ thermobarometer according to the calibration by [Huang and Audétat \(2012\)](#) ([Fig. 9](#)). The Ti uptake into quartz, under certain P-T conditions, depends on the Ti activity of the melt. Leucocratic granitic melts, usually free of rutile, will have the $a_{\text{Ti}} < 1$. [Drivenes et al. \(2016\)](#) set the approximate value of $a_{\text{Ti}} = 0.5$ for Cornish stanniferous granites, while

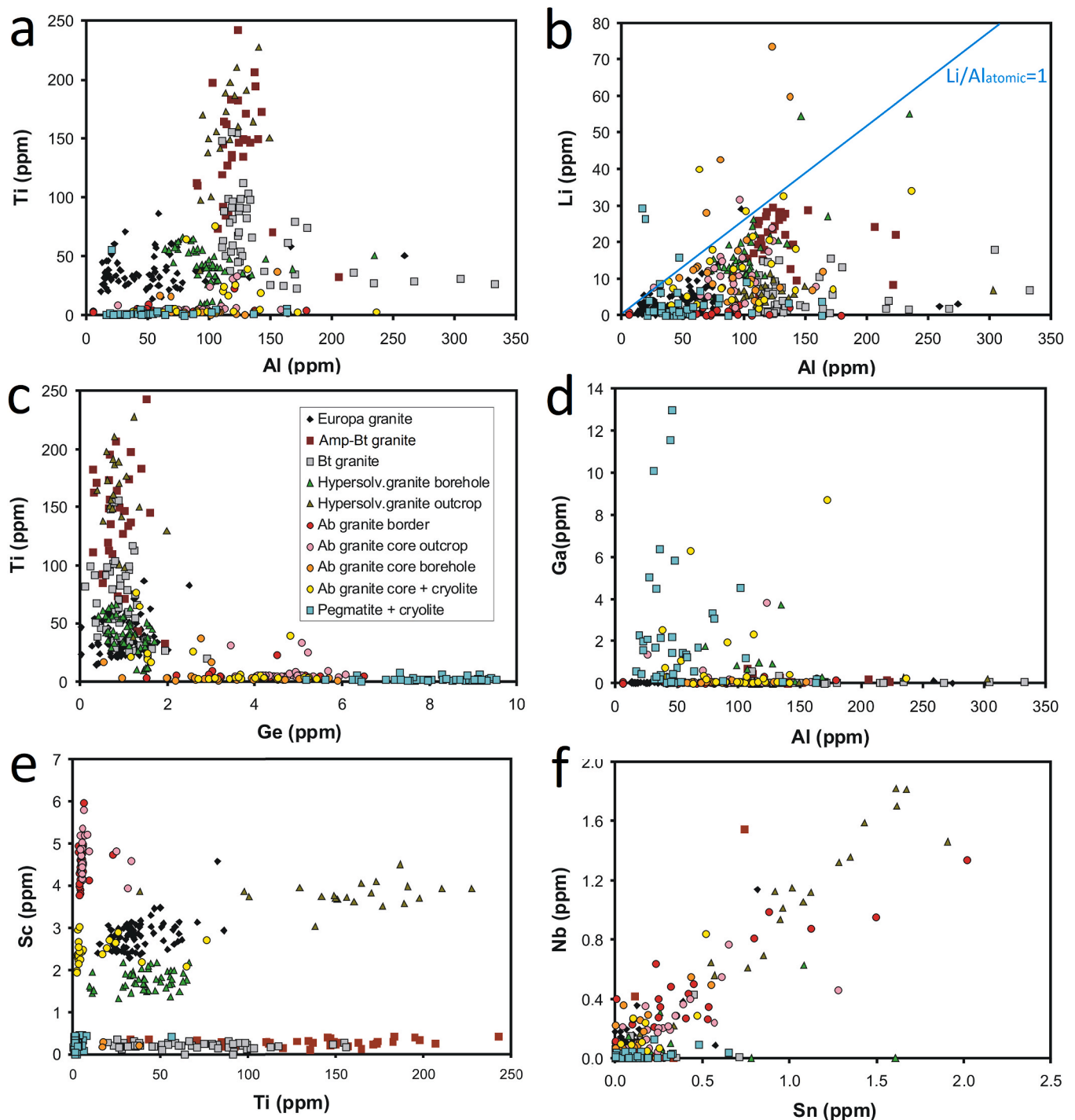


Fig. 6. Trace elements contents in quartz: a, Al vs. Ti; b, Al vs. Li; c, Ge vs. Ti; d, Al vs. Ga; e, Ti vs. Sc; f, Sn vs. Nb. The theoretical atomic ratio $Li/Al = 1$ is shown in fig. b.

values around 0.13–1 were proposed by Audéat (2013) for some rhyolites containing 0.03–0.12 wt% bulk TiO_2 . The calculation of more accurate values of a_{Ti} needs a possibility of independent determination of temperature or pressure, which is not available in our case. In addition, different proposed models give different solutions (see review in Kularatne and Audéat, 2014). For these reasons, the following P-T model estimation is only very approximate.

The Madeira biotite granite contains accessory rutile. Values of $a_{Ti} \sim 1$ can be supposed at the beginning of quartz crystallization (cores containing 92–149 ppm Ti), while the rims (25–66 ppm Ti) probably crystallized from a Ti-depleted melt at lower a_{Ti} . Assuming the subsolvus

character of the granite, i.e., crystallization at temperatures below 800 °C (Kroll et al., 1993), a model of biotite granite crystallization between ca. 700 and 650 °C at a nearly constant pressure of 3 kbar seems to be plausible (Fig. 9a).

The hypersolvus granite contains quartz with reverse Ti-zoning: 9.5–12 ppm in the cores and 40–53 ppm in the rims. This granite can be supposed to start crystallization at 800 °C or at somewhat higher temperature (Kroll et al., 1993). The rimwards increasing Ti-content is surprising at first glance, but similar evolution was already reported from the Teplice rhyolite, Czech Republic (Breiter et al., 2012), and from the Bandelier Tuff, New Mexico, USA (Audéat, 2013): Ti-increase

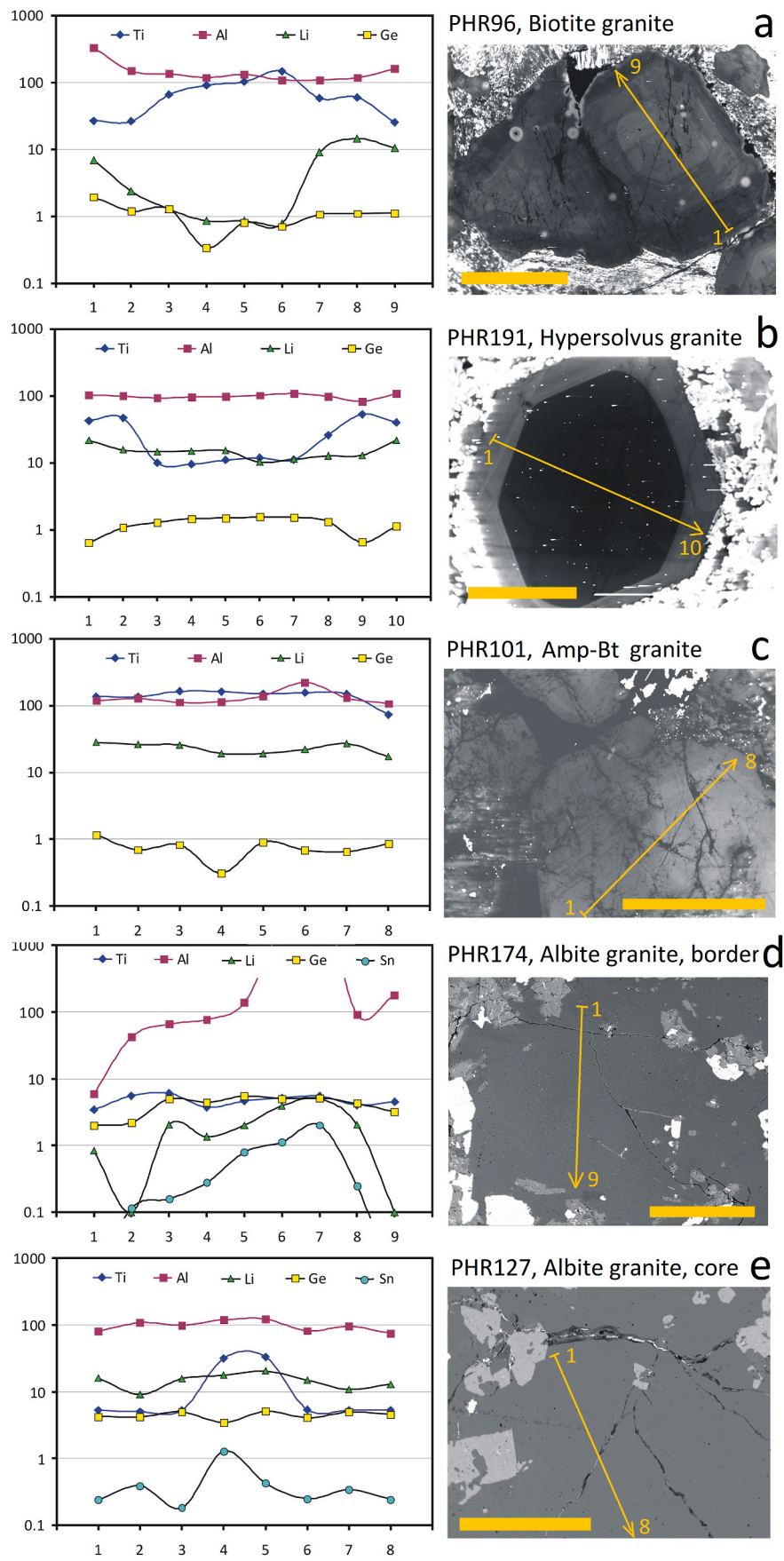


Fig. 7. Chemical and CL zoning of quartz from Madeira pluton: a, biotite granite (PHR-96); b, hypersolvus granite (PHR-191); c, amphibole-biotite granite (PHR-101); d, border facies of albite granite (PHR-174); e, core facies of albite granite (PHR-127). For interpretation of different styles of zoning see text.

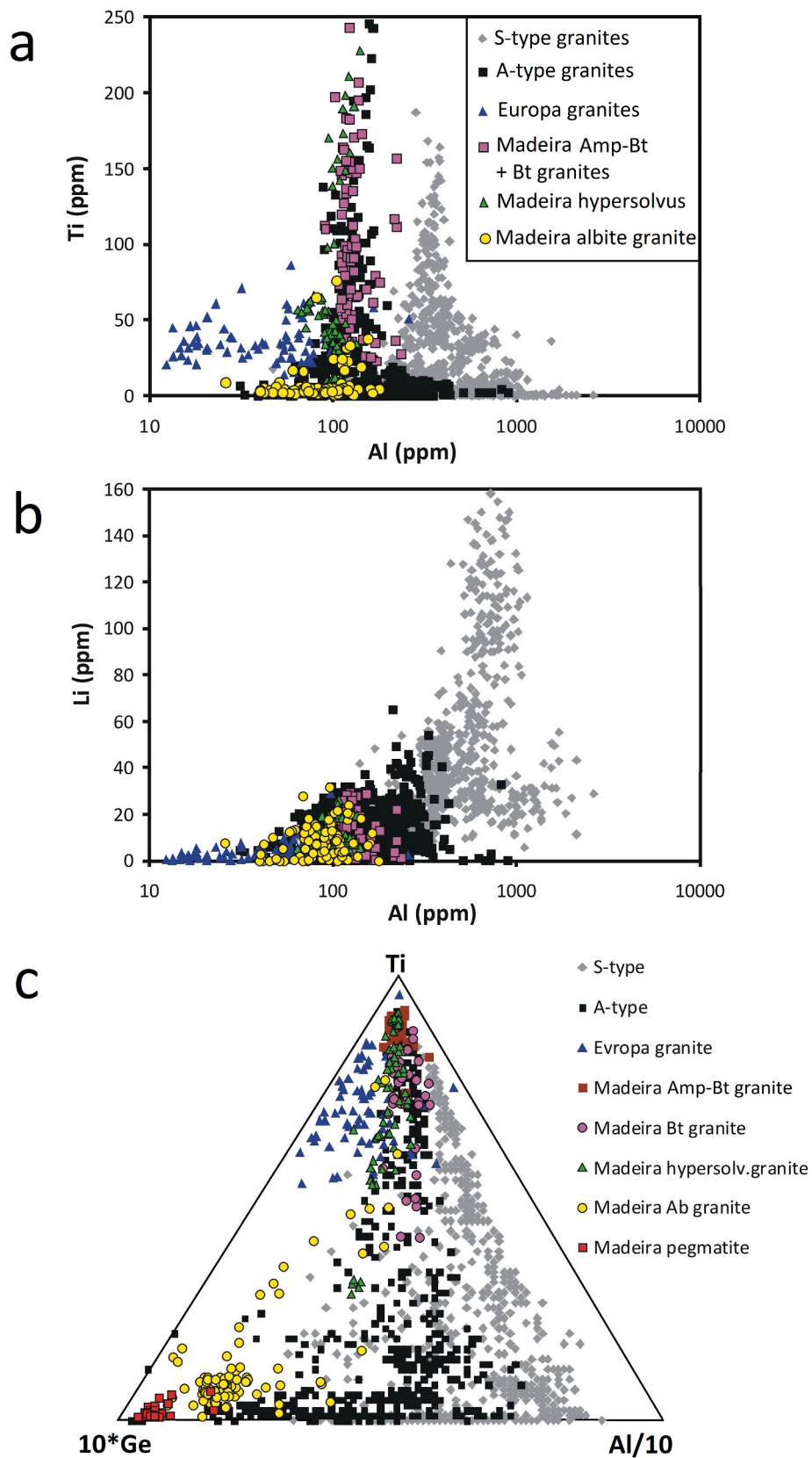


Fig. 8. Comparison of quartz from peralkaline and S- and A-type granites: a, Al vs. Ti; b, Al vs. Li; c, ternary plot Ti–Al/10–10*Ge, modified according to [Schrön et al. \(1988\)](#). Data for S- and A-type granites from [Breiter et al. \(2020\)](#).

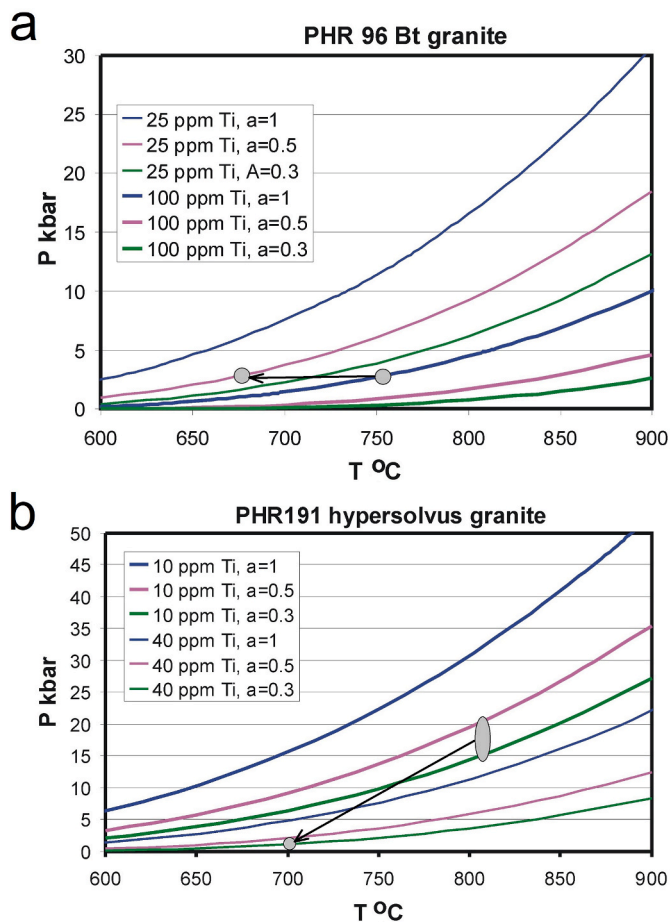


Fig. 9. Ti-in-quartz thermobarometer (TitaniQ acc. to Huang and Audétat, 2012): a, Madeira biotite granite (PHR-96); b, Madeira hypersolvus granite (PHR-191). For more detail see text.

during quartz fractionation can be explained by (i) increasing temperature, (ii) increasing a_{Ti} or (iii) decreasing pressure. The first two possibilities come to mind in case of rhyolites *via* a replenishment of magmatic reservoir with hot more basic portion of magma. In case of acid leucocratic granites, the third option, i.e. decrease of pressure due to fast emplacement is realistic. Thus, setting the a_{Ti} value to 0.3–0.5 (no Ti-oxides were found), we obtained the initial crystallization pressure in the range of 15–20 kbar and the end of crystallization at a temperature little below 700 °C and a pressure below 2 kbar (Fig. 9b).

5.3. Diversity of Madeira quartz chemistry: contribution to better constraints of pluton evolution?

A correct understanding of the relationship between all phases/granite types of a particular granite pluton constitutes a basis for a more detailed modeling of the evolution of granites and related mineralization. In the case of the Madeira pluton, i.e., the Pitinga tin-niobium-cryolite deposit, the space and time relations of some rocks are well constrained in terms of isotopic ages (Costi et al., 2000a), field relations (Costi et al., 2000a; Minuzzi et al., 2006), and geochemical characteristics (Horbe et al., 1991; Lenharo et al., 2003; Costi et al., 2005, 2009). The Pb–Pb ages of 1824 ± 2 and 1822 ± 2 Ma for the amphibole-biotite and biotite granites, respectively, together with a similar, generally less evolved geochemical composition define the relatively older, not mineralized stage of pluton origin. The compositions of quartz from these granite types support this idea: quartz is relatively rich in Ti (medians 147 and 66 ppm, respectively) with nearly identical contents of Al (124 and 127 ppm, respectively) and Ge (0.86 and 0.90 ppm,

respectively). Also rather primitive composition of zircon with low Hf-content (<0.02 apfu Hf, Nardi et al., 2012) supports such interpretation.

In the case of the hypersolvus granite, Costi et al. (2000a) found an age of 1818 ± 2 Ma, while the age of the border facies of the albite granite is only very roughly constrained at 1822 ± 22 Ma (Bastos Neto et al., 2014) due to the metasomatic alteration of zircons. In the core facies, Costi et al. (2000a) found only zircons with high contents of common Pb. Nevertheless, based on a detailed study of the contacts between the above mentioned granites, Costi et al. (2000a, 2009) interpreted the hypersolvus and albite granites to be contemporaneous: mingling of the two rock types was documented in boreholes in the central part of the pluton, although a sharp and transitional contacts were found in outcrops. Moreover, the pericontact part of the albite granite was hydrothermally altered (“border facies”) – another feature limiting our abilities to recognize contact relations with a higher certainty. Thus, the material relationship between the hypersolvus and albite granites, i.e., their possible relation *via* magmatic fractionation, remains unclear. Quartz from the outcropping hypersolvus granite is CL-free, rich in Ti and poor in Li, i.e., chemically similar to the neighboring amphibole-biotite granite. Moreover, it is enriched in Sn and Nb, which may indicate some re-equilibration with hydrothermal fluid escaping from the albite granite. In contrast, quartz from the deep-seated hypersolvus granite is strongly zoned in CL, which is, together with its chemical composition, similar to the Madeira biotite granite. Therefore, the texture and the composition of quartz do not support magmatic relations of the hypersolvus granite and the albite granites *via* magmatic fractionation. On the other side, two major zones with veins and pods mainly composed of cryolite, developed along a complex alternation of layers of albite granite and hypersolvus granite, in the inner part of the pluton (Fig. 2b), suggests that both granites were mingled and later exposed to similar metasomatic processes.

6. Conclusions

The main achievements of the present study can be summarized as follows:

1. Compared to quartz from peraluminous rare-metal granites, quartz from the studied alkaline granites of the Pitinga area is poorer in alumina ($\text{Al} < 150$ ppm) and lithium (mostly $\text{Li} < 20$ ppm). Progressive magmatic differentiation is expressed in a strong decrease in Ti (from 200 to <5 ppm) and a concurrent enrichment in germanium (max. 10 ppm Ge), scandium (max. 6 ppm Sc), and gallium (max. 5 ppm Ga). Typical features of quartz from peralkaline rocks are well constrained in the Ti–Al–Ge ternary diagram, forming an array along the Ti–Ge join.

2. Based on the TitaniQ thermobarometer with a calibration by Huang and Audétat (2012), the Madeira biotite granite crystallized between ca. 700 and 650 °C at a nearly constant pressure of 3 kbar. The hypersolvus granite is inferred to started to crystallize at 800 °C and 15–20 kbar, and the crystallization finished at a temperature little below 700 °C and a pressure below 2 kbar.

3. New textural and chemical data on quartz are in agreement with previous geochronological data (Costi et al., 2000a): the Madeira pluton comprises two older pulses of less evolved, mostly metaluminous amphibole-biotite and biotite granites, and two younger pulses of mutually mingled metaluminous hypersolvus and peralkaline albite granites. The texture and the composition of quartz do not support direct magmatic relations between the hypersolvus granite and the albite granite *via* magmatic fractionation, but these two granites were later exposed to similar metasomatic processes.

Credit author statement

Karel Breiter: Writing – original draft, Visualization, Methodology, Investigation, Conceptualization. **Hilton Tulio Costi:** Writing – original draft, Investigation. **Michaela Vašinová Galiová:** Supervision,

Methodology. Michaela Hložková: Data curation. Jindřich Kynický: Funding acquisition. Zuzana Korbelová: Data curation. Marek Dosbaba: Methodology, Data curation.

Declaration of competing interest

The authors declare that they have no known competing financial interests or personal relationships that could have appeared to influence the work reported in this paper.

Data availability

Data will be made available on request.

Acknowledgements

This study was supported by the Czech Science Foundation, project No. EXPRO 19–29124X to BIC Brno. Cooperation of Z.K. was supported by RVO 67985831 of the Institute of Geology of the Czech Academy of Sciences. A detailed and inspirational review by one anonymous reviewer is acknowledged with thanks.

Appendix A. Supplementary data

Supplementary data associated with this article can be found, in the online version, at <https://doi.org/10.1016/j.jsames.2022.104025>.

References

- Audétat, A., 2013. Origin of Ti-rich rims in quartz phenocrysts from the Upper Bandelier Tuff and the Tunnel Spring Tuff, southwestern USA. *Chem. Geol.* 360–361, 99–104.
- Bastos Neto, A.C., Pereira, V.P., de Lima, E.F., 2005. A jazida de criolita da mina Pitinga (Amazonas). In: Marini, O.J., Queiroz, E.T., Ramos, B.W. (Eds.), *Caracterização de depósitos minerais da Amazonia*. DNP/CT-MINERAL-ADIMB, Brasília, pp. 481–552 (in Portuguese).
- Bastos Neto, A.C., Pereira, V.P., Ronchi, L.H., Lima, E.F., Frantz, J.C., 2009. The world-class Sn, Nb, Ta, F (Y, REE, Li) deposit and the massive cryolite associated with the albite-enriched facies of the Madeira A-type granite, Pitinga mining district, Amazonas State, Brazil. *Can. Mineral.* 47, 1329–1357.
- Bastos Neto, A.C., Ferron, J.T.M.M., Chauvet, A., Chemale, F., Lima, E.F., Barbanson, L., Costa, C.F.M., 2014. U–Pb dating of the Madeira Suite and structural control of the albite-enriched granite at Pitinga (Amazonia, Brazil): evolution of the A-type magmatism and implications for the genesis of the Madeira Sn–Ta–Nb (REE, cryolite) world-class deposit. *Precambrian Res.* 243, 181–196.
- Bettencourt, J.S., Juliani, C., Xavier, R.P., 8 others, 2016. Metallogenic system associated with granitoid magmatism in the Amazonian Craton: an overview of the present level of understanding and exploration significance. *J. S. Am. Earth Sci.* 68, 22–49.
- Beurlen, H., Müller, A., Silva, D., da Silva, M.R.R., 2011. Petrogenetic significance of LA-ICP-MS trace-element data on quartz from the Borborema pegmatite province, northeast Brazil. *Mineral. Mag.* 75, 2703–2719.
- Breiter, K., Müller, A., 2009. Evolution of rare-metal granitic magmas documented by quartz chemistry. *Eur. J. Mineral.* 21, 335–346.
- Breiter, K., Svojtka, M., Ackerman, L., Švecová, K., 2012. Trace element composition of quartz from the Variscan Teplice caldera (Krušné hory/Erzgebirge Mts., Czech Republic/Germany): insights into the volcano-plutonic complex evolution. *Chem. Geol.* 326–327, 36–50.
- Breiter, K., Gardenová, N., Kanický, V., Vaculovič, T., 2013. Gallium and germanium geochemistry during magmatic fractionation and post-magmatic alteration in different types of granitoids: a case study from the Bohemian Massif, Czech Republic. *Geol. Carpathica* 64, 171–180.
- Breiter, K., Durišová, J., Hrstka, T., Korbelová, Z., Hložková Vaňková, M., Vašinová Galiová, M., Kanický, V., Rambousek, P., Kněsl, I., Dobeš, P., Dosbaba, M., 2017. Assessment of magmatic vs. metasomatic processes in rare-metal granites: a case study of the Čínovec/Zinnwald Sn–W–Li deposit, Central Europe. *Lithos* 292–293, 198–217.
- Breiter, K., Durišová, J., Dosbaba, M., 2020. Chemical signature of quartz from S- and A-type rare-metal granites – a summary. *Ore Geol. Rev.* 125, 103674.
- Borges, R.M.K., Villas, R.N.N., Fuzikawa, K., Dall'Agnol, R., Pimenta, M.A., 2009. Phase separation, fluid mixing, and origin of the greisens and potassic episyenite associated with the Água Boa pluton, Pitinga tin province, Amazonian Craton, Brazil. *J. S. Am. Earth Sci.* 27, 161–183.
- Borges, R.M.K., Amorim, L.E.D., Rios, F.J., dos Santos, G.C.S., Freitas, M.E., de Lima, T.A.F., Santos, A., Pedrosa, T.A., 2021. Melt–melt immiscibility and implications for the origin of Madeira albite-rich granite, Pitinga mine, Amazonas, Brazil: a melt inclusion study. *Braz. J. Geol.* 51 (4), e20210011.
- Costi, H.T., Dall'Agnol, R., Moura, C.A.V., 2000a. Geology and Pb–Pb geochronology of Paleoproterozoic volcanic and granitic rocks of Pitinga province, Amazonian craton, northern Brazil. *Int. Geol. Rev.* 42, 832–849.
- Costi, H.T., Horbe, A.M.C., Borges, R.M.K., Dall'Agnol, R., Rossi, A., Sighnolfi, G., 2000b. Mineral chemistry of cassiterites from Pitinga province, Amazonian craton, Brazil. *Rev. Bras. Geociências* 30, 775–782.
- Costi, H.T., Dall'Agnol, R., Borges, R.M.K., Minuzzi, O.R.R., Teixeira, J.T., 2002. Tin-bearing sodic episyenites associated with the Proterozoic, A-type Água Boa granite, Pitinga mine, Amazonian craton, Brazil. *Gondwana Res.* 5, 435–451.
- Costi, H.T., Borges, R.M., Dall'Agnol, R., 2005. Depósitos de estanho da mina Pitinga, estado do Amazonas. In: Marini, O.J., Queiroz, E.T., Ramos, B.W. (Eds.), *Caracterização de depósitos minerais da Amazonia*. DNP/CT-MINERAL-ADIMB, Brasília, pp. 391–475 (in Portuguese).
- Costi, H.T., Dall'Agnol, R., Pichavant, M., Ramo, O.T., 2009. The peralkaline tin-mineralized Madeira cryolite albite-rich granite of Pitinga, Amazonian craton, Brazil: petrography, mineralogy and crystallization processes. *Can. Mineral.* 47, 1301–1327.
- Drivenes, K., Larsen, R.B., Müller, A., Sorensen, B.E., 2016. Crystallization and uplift path of late Variscan granites evidenced by quartz chemistry and fluid inclusions: example from the Lands'End granite, SW England. *Lithos* 252–253, 57–75.
- European Commission, 2020. Critical Raw Materials Resilience: Charting a Path towards Greater Security and Sustainability.
- Ferron, J.M.T.M., Bastos Neto, A.C., Lima, E.F., Nardi, L.V.S., Costi, H.T., Pierosan, R., Prado, M., 2010. Petrology, geochemistry, and geochronology of Paleoproterozoic volcanic and granitic rocks (1.89–1.88 Ga) of the Pitinga province, Amazonian craton, Brazil. *J. S. Am. Earth Sci.* 29, 483–497.
- Garate-Olave, I., Müller, A., Roda-Robles, E., Gil-Grespo, P.P., Pesquera, A., 2017. Extreme fractionation in a granite-pegmatite system documented by quartz chemistry: the case study of Tres Arroyos (Central Iberian Zone, Spain). *Lithos* 286–287, 162–174.
- Götze, J., 2009. Chemistry, textures and physical properties of quartz – geological interpretation and technical application. *Mineral. Mag.* 73, 645–671.
- Götze, J., Pan, Y., Müller, A., 2021. Mineralogy and mineral chemistry of quartz: a review. *Mineral. Mag.* 85, 639–664.
- Gourcerol, B., Gloaguen, E., Melleton, J., Tuduri, J., Galiegue, X., 2019. Re-assessing the European lithium resource potential – a review of hard-rock resources and metallogeny. *Ore Geol. Rev.* 109, 494–519.
- Hadlich, I.W., Bastos Neto, A.C., Botelho, N.F., Pereira, V.P., 2019. The thorite mineralization in the Madeira Sn–Nb–Ta world-class deposit (Pitinga, Brazil). *Ore Geol. Rev.* 105, 445–466.
- Harlaux, M., Kouzmanov, K., Gialli, S., Clark, A.H., 11 others, 2021. The upper Oligocene San Rafael intrusive complex (Eastern Cordillera, southeast Peru), host of the largest-known high-grade tin deposit. *Lithos* 400–401, 106409.
- Horbe, M.A., Horbe, A.C., Costi, H.T., Teixeira, J.T., 1991. Geochemical characteristic of cryolite-tin-bearing granites from the Pitinga mine, northwestern Brazil – a review. *J. Geochim. Explor.* 40, 227–249.
- Hreus, S., Výravský, J., Cempírek, J., Breiter, K., Vašinová Galiová, M., Krátký, O., Šešulka, V., Škoda, R., 2021. Scandium distribution in the world-class Li–Sn–W Čínovec greisen-type deposit: result of a complex magmatic to hydrothermal evolution, implications for scandium valorization. *Ore Geol. Rev.* 139, 104433.
- Hrstka, T., Gottlieb, P., Skála, R., Breiter, K., Motl, D., 2018. Automated mineralogy and petrology – applications of TESCANA integrated mineral analyzer (TIMA). *J. Geosci.* 63, 47–63.
- Huang, R., Audétat, A., 2012. The titanium-in-quartz (TitaniQ) thermobarometer: a critical examination and re-equilibration. *Geochimica et Cosmochimica Acta* 84, 75–89.
- Jacamon, F., Larsen, R.B., 2009. Trace element evolution of quartz in the charnockitic Kleivan granite, SW Norway: the Ge/Ti ratio of quartz as an index of igneous differentiation. *Lithos* 107, 281–291.
- Kovalenko, V.I., Yarmoluyk, V.V., Salnikova, E.B., Kozlovsky, A.M., Kotov, A.B., Kovach, V.P., Savatenkov, V.M., Vladykin, N.V., Ponomarchuk, V.A., 2006. Geology, geochronology, and geodynamics of the Khan Bogd alkali granite pluton in southern Mongolia. *Geotectonics* 40 (6), 450–466.
- Kroll, H., Evangelakakis, C., Voll, G., 1993. Two-feldspar geothermometry: a review and revision for slowly cooled rocks. *Contrib. Mineral. Petrol.* 114, 510–518.
- Kularatne, K., Audétat, A., 2014. Rutile solubility in hydrous rhyolite melts at 750–900 °C and 2 kbar, with application to titanium-in-quartz (TitaniQ) thermobarometry. *Geochim. Cosmochim. Acta* 125, 196–209.
- Larsen, R.B., Henderson, I., Ihlen, P.M., 2004. Distribution and petrogenetic behavior of trace elements in granitic pegmatite quartz from South Norway. *Contrib. Mineral. Petrol.* 147, 615–628.
- Lenharo, S.L.R., Moura, M.A., Botelho, N.F., 2002. Petrogenetic and mineralization processes in Paleo- to Mesoproterozoic rapakivi granites: example from Pitinga and Goiás, Brazil. *Precambrian Res.* 119, 277–299.
- Lenharo, S.L.R., Pollard, P.J., Born, H., 2003. Petrology and textural evolution of granites associated with tin and rare-metals mineralization at the Pitinga mine, Amazonas, Brazil. *Lithos* 66, 37–61.
- Marignac, C., Cuney, M., Cathelineau, M., Lecomte, A., Carocci, E., Pinto, F., 2020. The Panasqueira rare metal granite suite and their involvement in the genesis of the world-class Panasqueira W–Sn–Cu vein deposits: a petrographic, mineralogical, and geochemical study. *Minerals* 10, 562.
- Minuzzi, O.R.R., Bastos Neto, A.C., Flores, J.A.A., Pereira, V.P., Ferron, J.T.M.M., 2006. O depósito criolítico maciço e o minério disseminado de criolita da mina Pitinga (Amazonas, Brasil). *Rev. Bras. Geociências* 36, 104–123 (in Portuguese).
- Monnier, L., Lach, P., Salvi, S., Melleton, J., Bailly, L., Béziat, D., Monnier, Y., Gouy, S., 2018. Quartz trace-element composition by LA-ICP-MS as proxy for granite

- differentiation, hydrothermal episodes, and related mineralization: the Beauvoir granite (Echassières district), France. *Lithos* 320–321, 355–377.
- Monnier, L., Melleton, J., Vanderhaeghe, O., Salvi, S., Lach, P., Bruguier, O., Benmammour, A., Bailly, L., Béziat, D., Gloaguen, E., 2021. Episodic precipitation of wolframite during an orogen: the Echassières district, Variscan belt of France. *Minerals* 11, 923.
- Müller, A., Breiter, K., Seltmann, R., Pécskay, Z., 2005. Quartz and feldspar zoning in the eastern Erzgebirge volcano-plutonic complex (Germany, Czech Republic): evidence of multiple magma mixing. *Lithos* 80, 201–227.
- Müller, A., Herklotz, G., Giegling, H., 2018. Chemistry of quartz related to the Zinnwald/Cínovec Sn-W-Li greisen-type deposit, Eastern Erzgebirge, Germany. *J. Geochem. Explor.* 190, 357–373.
- Müller, A., Keyser, W., Simmons, W.B., Webber, K., Wise, M., Beurlen, H., Garate-Olave, I., Roda-Robles, E., Galliski, M.A., 2021. Quartz chemistry of granitic pegmatites: implications for classification, genesis and exploration. *Chem. Geol.* 584, 120507.
- Nardi, L.V.S., Formoso, M.L.L., Jarvis, K., Oliveira, L., Bastos Neto, A.C., Fontana, E., 2012. REE, Y, Nb, U, and Th contents and tetrad effect in zircon from a magmatic-hydrothermal F-rich system of Sn-rare metal-cryolite mineralized granites from the Pitinga Mine, Amazonia, Brazil. *J. S. Am. Earth Sci.* 33, 34–42.
- Paludo, C.M., Bastos Neto, A.C., Pereira, V.P., Botelho, N.F., 2018. Mineralogia e geoquímica de pegmatitos ricos em ETR, F e metais alcalinos associados a facies albíta granito no depósito de Sn-Nb-Ta- (F, ETR, U, Th) Madeira (mina Pitinga, AM, Brasil). *Pesqui. em Geociencias* 45, e0747.
- Perny, B., Eberhardt, P., Ramseyer, K., Mullis, J., Pankrath, R., 1992. Microdistribution of Al, Li, and Na in α quartz: possible causes and correlation with short-lived cathodoluminescence. *Am. Mineral.* 77, 534–544.
- Rusk, B.G., Reed, M.H., Dilles, J.H., Kent, A.J.R., 2006. Intensity of quartz cathodoluminescence and trace-element content in quartz from the porphyry copper deposit at Butte, Montana. *Am. Mineral.* 91, 1300–1312.
- Rusk, B.G., Lowers, H.A., Reed, M.H., 2008. Trace elements in hydrothermal quartz: relationship to cathodoluminescence textures and insights into vein formation. *Geology* 36, 547–550.
- Santos, J.O.S., Hartmann, L.A., McNaughton, N.J., Fletcher, I.R., 2002. Timing of mafic magmatism in the Tapajós Province (Brazil) and implications for the evolution of the Amazon Craton: evidence from baddeleyite and zircon U–Pb SHRIMP geochronology. *J. S. Am. Earth Sci.* 15, 409–429.
- Schrön, W., Schmädicke, E., Thomas, R., Schmidt, W., 1988. Geochemische Untersuchungen an Pegmatitquarzen. *Zeitschrift fuer geologische Wissenschaften* 16, 229–244.
- Schulz, K.J., DeYoung Jr., J.H., Seal, R.R., II Bradley, D.C., 2017. Critical Mineral Resources of the United States—Economic and Environmental Geology and Prospects for Future Supply. U.S. Geological Survey Professional Paper 1802, pp. 1–797.
- Schwartz, M.O., 1992. Geochemical criteria for distinguishing magmatic and metasomatic albite-enrichment in granitoids – examples from the Ta-Li granite Yichun (China) and the Sn-W deposit Tikus (Indonesia). *Miner. Deposita* 27, 101–108.
- Shi, C., Yan, M., Chi, Q., 2011. Abundances of chemical elements in granitoids of different geological ages and their characteristic in China. *Geosci. Front.* 2, 261–275.
- Thomas, J.B., Watson, E.B., Spear, F.S., Shemella, P.T., Nayak, S.K., Lanzorotti, A., 2010. TitaniQ under pressure: the effect of pressure and temperature on the solubility of Ti in quartz. *Contrib. Mineral. Petrol.* 160, 743–759.